Comparison of a Core Disruptive Accident simulation with the MARS experimental test

Marie-France Robbe, Jean-Yves Cariou, Eloi Treille, Michel Lepareux

▶ **To cite this version:**

Marie-France Robbe, Jean-Yves Cariou, Eloi Treille, Michel Lepareux. Comparison of a Core Disruptive Accident simulation with the MARS experimental test. International Conference on Numerical Methods in Continuum Mechanics 2000, Sep 2000, Liptovsky Jan, Slovakia. cea-04177342

HAL Id: cea-04177342

https://cea.hal.science/cea-04177342v1

Submitted on 4 Aug 2023

HAL is a multi-disciplinary open access archive for the deposit and dissemination of scientific research documents, whether they are published or not. The documents may come from teaching and research institutions in France or abroad, or from public or private research centers.

L'archive ouverte pluridisciplinaire **HAL**, est destinée au dépôt et à la diffusion de documents scientifiques de niveau recherche, publiés ou non, émanant des établissements d'enseignement et de recherche français ou étrangers, des laboratoires publics ou privés.

Comparison of a Core Disruptive Accident simulation with the MARS experimental test

M.F. Robbe
CEA Saclay, DRN-DMT-SEMT, 91191 Gif sur Yvette cedex, France
Tel: (33) 1 69 08 87 49, Fax: (33) 1 69 08 52 42, E-mail: mfrobbe@cea.fr
Y. Cariou
Novatome, NVPM, 10 rue Juliette Récamier, 69006 Lyon, France
E. Treille
Socotec Industrie, 1 av. du Parc, 78180 Montigny le Bretonneux, France
M. Lepareux
CEA Saclay, DRN-DMT-SEMT, 91191 Gif sur Yvette cedex, France

Abstract

In case of a Hypothetical Core Disruptive Accident (HCDA) in a Liquid Metal Reactor, the interaction between fuel and liquid sodium creates a high pressure gas bubble in the core. The violent expansion of this bubble loads the vessel and the internal structures, whose deformation is important. The experimental test MARS simulates a HCDA in a small scale mock-up containing all the significant internal components of a Fast Breeder Reactor. The test-facility is filled with water topped by an argon blanket and the explosion is generated by an explosive charge.

This paper presents a numerical simulation of the test with the CASTEM-PLEXUS code. The top closure is represented by massive structures. The main internal structures are described by shells while the peripheral massive structures are taken into account with a pressure loss because their geometry is too complicated to mesh them. The computed results are compared to the experimental results and the ones obtained in a previous numerical simulation with the CASTEM-PLEXUS code.

1 INTRODUCTION

In case of a Hypothetical Core Disruptive Accident (HCDA) in a Liquid Metal Reactor, the interaction between fuel and liquid sodium creates a high pressure gas bubble in the core. The violent expansion of this bubble loads the vessel and the internal structures, whose deformation is important.

During the 70s and 80s, the LMFBR integrity was studied with codes specially devoted to the analysis of transient loads resulting from a HCDA : PISCES 2 DELK (Cowler, 1979), REXCO (Chang, 1974), MICE, ICECO, ICEPEL, STRAW and SADCAT (Chang, 1977), SURBOUM (Stiévenart, 1975), SEURBNUK/EURDYN (Cameron, 1977) (Smith, 1983) (Smith, 1987), ASTARTE (Cigarini, 1983), CASSIOPEE (Graveleau, 1979), SIRIUS...

In order to validate these codes, experimental programmes and benchmarks were undertaken by several countries : COVA (Hoskin, 1978) (Holtbecker, 1977) (Albertini, 1984) (Wenger, 1987) (Kendall, 1980), APRICOT (West, 1980), WINCON (Sidoli, 1988), STROVA (Kendall, 1986), CONT (Benuzzi, 1987), MARA...

The french code SIRIUS (Blanchet, 1981) (Daneri, 1981) (Acker, 1981) was validated on the french experimental programme MARA (Louvet, 1989) (Bour, 1989). Based on a 1/30 scale model of the Superphenix reactor, the French programme MARA-MARS involved eleven tests of gradual complexity due to the addition of internal deformable structures:

• MARA 1 and 2 considered a vessel partially filled with water and closed by a rigid roof (Acker, 1981),

- MARA 4 represented the main core support structures (Smith, 1985),
- MARA 8 and 9 were closed by a flexible roof (Fiche, 1985),
- MARA 10 included the core support structures (CSS) and a simplified representation of the above core structure (ACS) (Louvet, 1987).

The MARS test (Falgayrettes, 1983) rested on a 1/20 scale mock-up including all the significant internal components.

As other codes using a Lagrangian approach, SIRIUS needed rezonings during calculation because the internal structure presence caused high distortion of the fluid meshes. Finite differences were used for the sodium and the roof and finite elements for the thin vessel. As the argon and the bubble were not meshed, a law related volume to pressure.

At the end of the 80s, it was preferred to add a specific HCDA sodium-bubble-argon tri-component constitutive law (Lepareux, 1991) to the general ALE fast dynamics finite element CASTEM-PLEXUS code. The HCDA constitutive law was qualified (Casadei, 1989) on the CONT benchmark.

In order to demonstrate the CASTEM-PLEXUS capability to predict the behaviour of real reactors (Lepareux, 1993) (Cariou[a], 1997), axisymmetric computations of the MARA series were confronted with the experimental results. The computations performed at the beginning of the 90s showed a rather good agreement between the experimental and computed results for the MARA 8 and MARA 10 tests even if there were some discrepancies (Cariou, 1993). On the contrary, the prediction of the MARS structure displacements and strains was overestimated (Cariou[b], 1997).

As the process used for dealing with the fluid-structure coupling was improved since then and as this process improved the precision of the results for the tests MARA8 and MARA10, it was undertaken another comparison between the experimental results of the MARS test with a finer size of the mesh.

This paper presents the numerical simulation of the MARS test with the CASTEM-PLEXUS code. The top closure is represented by massive structures. The main internal structures are described by shells while the peripheral massive structures are taken into account with a pressure loss because their geometry is too complicated to mesh them. The computation uses the new process for the fluid-structure treatment. After a brief presentation of the MARS test-facility, the paper is focused on the numerical models, the analysis of the results computed by the code CASTEM-PLEXUS and a comparison with the experimental results and the previous numerical results computed by CASTEM-PLEXUS.

2 DESCRIPTION OF THE MARS TEST-FACILITY

The primary circuit of the Superphenix reactor (Fig. 1) is a "pool" design (NERSA, 1987). The whole core, primary pumps and intermediate heat exchangers are enclosed in the main reactor vessel which is made of stainless steel and welded to the roof slab. The main reactor vessel is encased in a safety vessel also made of stainless steel.

The MARS experiment (Fig. 2) was realised at the CEA-Cadarache in order to simulate a HCDA in a 1/20 scale mock-up of the Superphenix reactor block. The main vessel (1 m diameter and 1 m height) includes all the significant internal components of the reactor (Falgayrettes, 1983).

The main vessel, of variable thickness (0.8 to 1.6 mm), was an assembly of a cylindrical part and of a two part torospherical bottom. The cylindrical part was made of 316L stainless steel whereas the bottom was made of 304L stainless steel. The two inner vessels were modelled, as

well as the anti-convecting device and the main vessel cooling system.

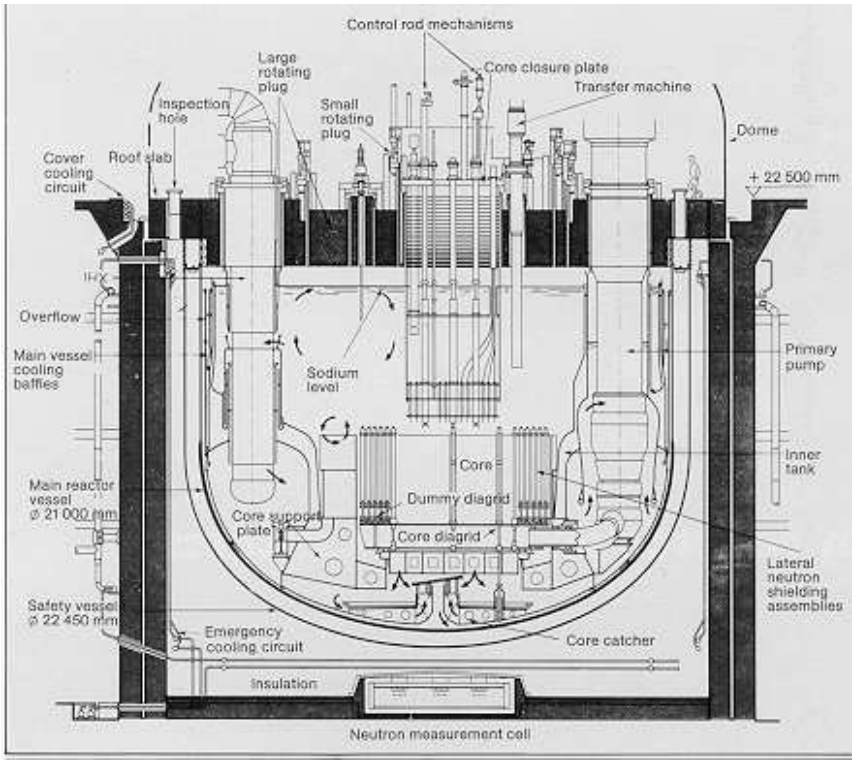

Fig. 1: The Superphenix reactor

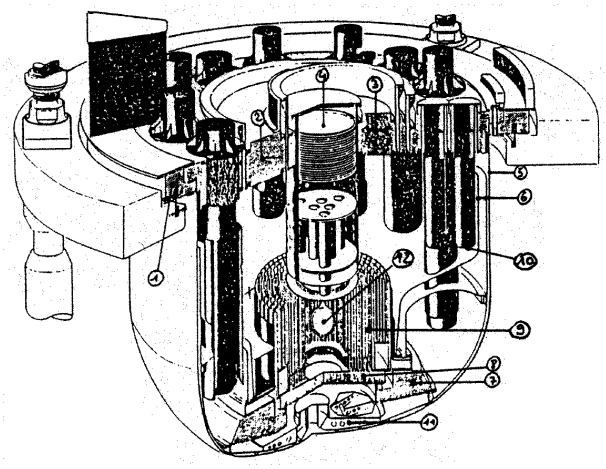

mark 1: roof
mark 2: large rotating plug
mark 3: small rotating plug
mark 4: core cover plug
mark 5: main vessel
mark 6: internal vessels
mark 7: core support structures
mark 8: diagrid support
mark 9: core and neutron shieldings
mark 10: pumps and heat exchangers
mark 11: core catcher

Fig. 2: The MARS test-facility

The core cover plug was a rather complicated structure, despite simplifications compared with the reactor geometry: the model included the top plate, the in-pile shell with its pipes, the spacer plates and the heat-insulation. The core catcher was composed of the catcher plate, support structure, vertical flanges, chimney and spacing feet.

The lateral neutron shielding was represented by four radially split shells and their supporting structures. The mass of the unmelted part of the core was simulated by a mixing of aluminium cylinders and steel hexagons fixed into two AG3 aluminium plates. The strongback and the diagrid support were respectively represented by a non-axisymmetric ring and a cylinder.

The roof slab was constituted by two circular plates of different thickness to simulate the reactor roof stiffness. Openings were drilled to enable the passage of the large components and the two rotating plugs were concentrically off as in the reactor.

The main components inserted through the roof slab were modelled: four primary pumps, eight intermediate heat exchangers, four emergency cooling exchangers and two integrated purification devices. The various supporting rings (roof slab, core support structure, large components) and joining rings (between the roof slab and the rotating plugs) were represented.

The mass deficit of the mock-up cover simulation was compensated by lead plates providing additional weights on the cover. The safety vessel, the dome, the biological shield plates and the handling machine were represented only by their inertia using lead plates. Rubber-ring bands simulated the heat-insulating material between the roof and the main vessel and the gas intervals of the roof slab.

The thin structures (inner vessels, baffles, lateral neutron shielding, main components, emergency heat exchangers, core cover plug, core catcher, core, joining and supporting rings) were mainly made of 304L stainless steel in order to simulate the austenistic steel of the reactor structures. The massive structures and those made of heterogeneous materials (roof slab, rotating plugs, core support structure, diagrid support) were made of A5 aluminium. The top plate of the core cover plug was made of A42 aluminium.

The sodium coolant at operating conditions was simulated by water at 20°C. The cover gas of the mock-up was the same as in the reactor (argon).

The test was fired using a 80 g low density low pressure explosive charge of L54/16 composition (David, 1978). The charge mass was chosen to simulate the 800 MJ full scale mechanical energy release used in the reference HCDA in the Superphenix reactor. The explosive charge was supported by the base of the core cover plug.

The whole test was well instrumented with:
- 19 pressure transducers fitted on the roof slab and the rotating plugs,
- 5 accelerometers placed on the reactor cover,
- 24 strain gauges attached on the main vessel, roof slab support ring and cover joining rings,
- 3 high speed cameras used to obtain displacements of the main vessel, roof slab and large plug, small plug and core cover plug,
- residual deformations were evaluated by measuring, before and after the firing, mesh sizes of the grid drawn on the different structures.

3 NUMERICAL MODELING OF THE TEST-FACILITY

CASTEM-PLEXUS (Chavant, 1979) (Hoffmann, 1984) (Robbe, 1994) (Robbe[a], 1999) is a general fast dynamics finite element code devoted to the analysis of problems involving fast transients. It can deal with fluids and structures with a possibility of coupling. A specific CDA constitutive law was implemented in the code in order to be able to represent precisely this kind of explosion.

Owing to the symmetry of the mock-up, an axisymmetric representation was chosen for the numerical simulation of the MARS test-facility with the CASTEM-PLEXUS computer code. The external structures were modeled by shells or massive structures and the main internal structures were described with a classical shell model. The peripheral structures were globally taken into account by means of a pressure loss.

The model includes a representation of the main vessel with three thin shells of different thickness and made of different materials for the cylindrical part and the torospherical part of the vessel. The top of the test-facility is described by massive elements for the roof, the small rotating plug and the large rotating plug. The massive fixings hanging the test-facility to the rigid frame are represented by a cylindrical shell at the extremity of the roof.

The top closure is assimilated to an axisymmetric structure for the needs of the numerical simulation. The openings in the roof for the passage of the components (pumps, heat exchangers) are simply accounted for by the mass they remove to the roof. Local masses on the top of the roof and on the small and large rotating plugs are added to consider the mass of the instrumentation and of the lead plates compensating the mass deficit of the MARS mock-up in relation to the real reactor. The additional local mass at the centre of the roof top also includes the mass of the internal components (pumps, heat exchangers, purification devices). Another local mass is placed at the edge of the roof to simulate the lead plates used in the test-facility to describe the inertia of the safety vessel, the dome, the biological shield plates and the handling machine.

The core cover plug was simplified. The upper part is modeled by the top plate and three plates simulate the heat and neutronic insulation. The in-pile shell and the three spacer plates are also meshed. The pipes are assimilated to two cylinders. The external shell surrounding the plug is also represented.

The joining rings between the roof slab and the three plugs are formed, in the mock-up, by concentric and cylindrical plates linked by a bridle at their top extremity. They are represented with thin shells made of aluminium and joining the top of the massive structures. Complementary shell elements made of rubber and joining the base of the massive structures were added to prevent the going up of argon in the free slits.

The heat-insulating material between the roof and the main vessel is represented by an horizontal rubber-ring band joining the roof base to the main vessel and preventing the upwards motion of argon in the empty slit. The main vessel, hung to the roof in the MARS test-facility, is fixed rigidly to the roof in the numerical model.

In the centre of the test-facility, the strongback, the neutron shielding support, the support of the baffles and of the internal vessel being fitted together, they are described by a single rigid structure, that we will call the Core Support Structure (CSS). This structure is assimilated to an axisymmetric shell of constant thickness, allocating to it an equivalent mass corresponding to the mass of all the structures. The CSS is supposed to be rigid and to transmit the totality of the forces to the structures fixed on it. The CSS is attached to the vessel by a cylindrical collar.

The diagrid support is represented by a thin shell. The core is not meshed: it is simply taken into account by an added mass spread along the diagrid. The diagrid support is fixed to the core support structure by a swivel link. Concerning the four shells schematizing the neutron shielding in the MARS mock-up, only the central one is modeled. This shell governs the fluid port between the core cover plug and the neutron shielding. The three other shells are taken into account by a local added mass located at the base of the first neutron shielding shell.

The baffles surrounding the outer neutron shielding are assimilated to an axisymmetric structure and represented by a vertical shell. The internal vessel is composed of two shells. Only the central one is meshed; the second one is simply described by an additional local mass at the base of the meshed internal vessel. The shielding, the baffle shell, the internal vessel are embedded on the Core Support Structure.

The core catcher is not meshed because its complex geometry would impose a lot of shells of small dimensions and therefore a very fine local meshing, not compatible with the rest of the model. Consequently, the core catcher is represented by an added mass spreaded along the bottom of the main vessel.

The behaviour of the structures previously quoted is generally described with isotropic elastic-plastic constitutive laws. However elastic laws are used to describe the rubber elements of weak resistance joining the different parts of the roof and the plugs, the internal and medium cylinders schematizing the pipes of the core cover plug whose constitutive law is approximated by means of an homogenization of the non-axisymmetric structures. The core support structure behaviour is also supposed linear elastic.

The presence of the internal components (pumps and heat exchangers) are taken into account in a global way in both models. The components are represented by a pressure loss applied along a cylinder located at the average radius of the components. This pressure loss coefficient is estimated from (Idel'Cik, 1986) and by supposing that a cylindrical obstacle partially blocks up the port. The surface of this obstacle is given by the ratio between the solid section and the total section for a 1 radian angle.

The figure 3 and 4 present the complete mesh of the MARS test and the structure representation.

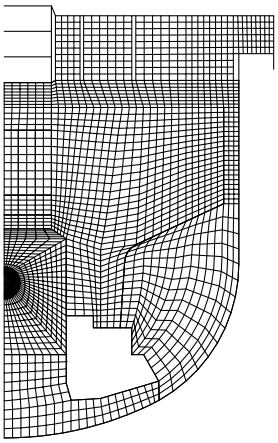

Fig. 3: Mesh of the MARS test

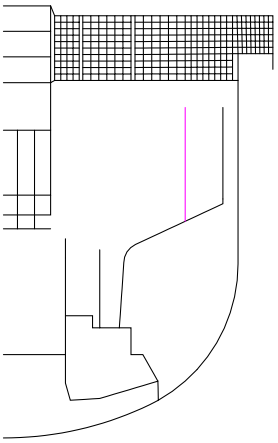

Fig. 4: Mesh of the structures

In case of a HCDA, the internal fluids are sodium, argon and a gas bubble. In the MARS test, the sodium and bubble are respectively replaced by water and an explosive charge. Water and argon are initially at the atmospheric pressure whereas the explosive charge induces an initial pressure of 288 MPa in the bubble area.

The characteristics taken into the numerical model are:

- Water : $\rho = 998.3$ kg/m^3 sound speed $C = 1550$ m/s $p^{(0)} = 10^5$ Pa
- Argon : $\rho = 1.658$ kg/m^3 $\lambda = c_p/c_v = 1.67$ $p^{(0)} = 10^5$ Pa
- Explosive charge : $\rho = 400$ kg/m^3 polytropic coef. $\eta = 1.322$ $\lambda = 1.24$ $p^{(0)} = 2.8810^8$ Pa

In CASTEM-PLEXUS, the fluids and solid structures can be described with an Eulerian, Lagrangian or A.L.E. (Arbitrary Lagrange Euler) approach. In the models, all the structures are represented with the lagrangian description and the mesh follows the deformation of the structures. The bubble zone is kept fixed. Indeed if the bubble grid was ALE, the mesh would deform very much because of the expansion of the bubble gas due to its very high initial pressure and this large deformation would entail numerical difficulties to carry out the computation. Moreover, the fixed bubble grid is used as a reference for the updating of the ALE surrounding mesh. The water and the argon are described with an ALE modeling: the fluid grid is updated according to the deformation of the neighbouring structures.

Two kinds of fluid-structure coupling are available in the CASTEM-PLEXUS code. Their main differences lie in the definition of the local normal vector used to write the coupling relations between the freedom degrees of the fluid and the solid. The first fluid-structure coupling (FS2D instruction) requires the definition of coupling elements by the user and imposes to the fluid nodes to have the same displacements as the structure nodes. However, there is no automatic actualisation of the ALE grid for the elements other than the ones on the coupled lines.

The second coupling (FSA instruction) goes without coupling elements; the code considers directly the fluid and solid nodes in contact and writes relations allowing a possible tangential movement of the fluid in relation to the structure. The FSA coupling is well adapted to complex

geometries but it often implies a user intervention to pilot the displacements of the fluid ALE grid.

The FSA coupling was adopted for the MARS test because the presence of the internal structures involved large local displacements of the fluid grid. In the previous CASTEM-PLEXUS computations (Cariou, 1997), the FS2D coupling was used because the FSA coupling was developed later. However, in the current model, a FS2D coupling persists in a local area.

As the diagrid is merely put down on the Core Support Structure and as both structures are not rigidly linked, the diagrid extremity is linked to the CSS by a swivel contact. Consequently, there are two different structure nodes at the same location (the one pertaining to the diagrid and the other to the CSS) whereas there is only one fluid node facing the two structure ones. This configuration cannot be processed by the FSA coupling. Therefore a FS2D coupling was settled down at the connection between the diagrid, the core support structure and the fluid between the radial shielding and the CSS.

The boundary conditions are:

- Complete blocking of the base of the fixing shell hanging the mock-up to the rigid frame,
- No rotation of all the nodes of the top closure at the intersection between the massive structures and the shells: links between the joining rings and the roof slab and the small and large rotating plugs, link between the roof and the main vessel top, links at the extremities of the heat-insulating material between the roof and the main vessel, link between the roof edge and the fixing shell,
- No horizontal displacement and no rotation of the structure nodes located on the symmetry axis (core cover plug, diagrid, vessel) and of the nodes of the plates simulating the heat and neutronic insulation of the core cover plug,
- No horizontal displacement of the fluid nodes on the symmetry axis,
- No horizontal displacement of the core support structure,
- Vertical displacement of the core support structure equal to the vertical displacement of the point at the intersection between the collar and the vessel,
- Same vertical displacement for the four plates simulating the heat and neutronic insulation of the core cover plug.

To link a shell to a massive structure, it is necessary to impose identical displacements for the nodes of the shell extremity and of the massive structure facing each other. Are concerned the diagrid and the CSS, the roof and the fixing shell, the roof and the main vessel, the joining rings of the top closure.

The FSA coupling cannot be used for the nodes at the top extremity of the neutron shielding and the baffle because the code cannot define the local normal vector to a point in an opened medium. Therefore the FSA coupling is used all along both shells except at the top extremity. Identical displacements are then imposed for the solid node at the top edge of the shell and the facing fluid node.

In order to help the code to calculate correctly the ALE mesh updating in the areas of high fluid speed or high pressure variations, the user has to define relations governing the local displacement of the mesh. Three governing lines were set up.

The first line imposes to the fluid nodes between the lower plate of the core cover plug and the neutron shielding top to stay aligned between both structure nodes during the displacement of the structures. This relation prevents a large deformation of the ALE grid due to the huge flow of the fluid going out from the central zone. Besides, this line is used as a reference for the updating of the fluid in the central zone.

Two lines impose to the fluid nodes between the lateral shielding top and the baffle and between the baffle and the internal vessel to stay aligned between the structure nodes. These lines prevent a distortion of the fluid mesh due the large local motions of the structures in that area.

Inside the core cover plug, there is no fluid-structure coupling defined between the internal structures of the plug and the fluid because the fluid can cross the pipes simulated by vertical cylinders. No fluid coupling is defined between the upper part of the external shell surrounding the plug and the fluid because this shell was perforated in the test-facility and fluid could pass from the plug to the rest of the mock-up. Consequently, in order to preserve a regular meshing inside the core cover plug, the fluid nodes on the vertical lines between the lower plate simulating the heat and neutronic insulation and the upper spacer plate have to stay aligned between the structure nodes of both plates.

4 DESCRIPTION OF THE RESULTS

In this part, we try to present a synthesis of the results computed with the current version of CASTEM-PLEXUS. Initially, all the fluids are at rest in the whole mock-up. The bubble gas located in the centre is at a pressure of 288 MPa. The argon layer laying just below the roof and the water filling the rest of the test-facility are at the atmospheric pressure.

The pressurised gas starts expanding since the beginning of the computation, thus inducing the propagation of a shock wave through the mock-up. At 0.06 ms, the shock wave impacts the lateral neutron shielding and the CCP in-pile shell. Both structures are submitted to stresses. The fluid in the central area is propelled towards the nearest structures with a speed of about 200 m/s, uniform in all the directions.

The shock wave hits the diagrid support, the baffle and the two lower CCP spacer plates at 0.1 ms and the internal vessel lower part at 0.14 ms. The bubble gas expands a little in the central area. The water out of the central zone is accelerated outwards. The bubble gas speed is around 120 m/s whereas the speed of the water in motion is between 20 and 40 m/s.

The structures in the pressurised area are submitted to stresses and start moving away. However there is one exception: because of the swivel link between the diagrid support and the Core Support Structure, the diagrid bends immediately and the stresses increase very little in the structure.

The shock wave impacts the upper CCP spacer plate and the main vessel bottom at 0.2 ms. The fluid in the central zone orients mainly towards the free space between the neutron shielding and the in-pile shell. The fluid rebounds against the diagrid and then orients towards the shielding which suffers a local radial displacement a little above its base.

In the rest of the mock-up, the fluid continues its spherical expansion. Radial displacements and plastic strains are observed in the shielding and the baffle. Vertical displacements and plastic strains are noted in the lower part of the CCP and in the diagrid.

Between 0.22 and 0.4 ms, the shock wave splashes along the main vessel in the area filled with water, at the bottom under the diagrid as well as in the torospherical and cylindrical parts from the collar junction to the top. The bubble gas goes on expanding in the central area. The water is still accelerated outwards and impacts almost all the structures.

Two structure areas are protected: the main vessel below the CSS because the water cannot flow directly in the space between both structures, and the roof because of the presence of the argon layer. The argon layer is compressed upwards and pushed towards the corner joining the roof to the main vessel.

The majority of the internal structures suffers deformations : the neutron shielding, the baffle and the internal vessel bend slightly above their base, the diagrid support bends as well as the part of the main vessel located just under the diagrid. In the CCP, the in-pile shell being pushed up, the CCP vertical cylinders impose a bending to the spacer plates. Besides, the intermediate and external CCP cylinders suffer buckling in their lower part.

From 0.4 to 1 ms, the shock wave ends impacting the main vessel cylindrical part and then the pressurised water area goes down along the vessel until the collar junction. The bubble gas continues expanding in the central zone and it arrives at the free space between the neutron shielding and the in-pile shell. In the rest of the mock-up, the water is hurled spherically: all the structures are submitted to the water impact. The argon flows horizontally along the top closure towards the main vessel. All the shell structures (others than the top closure) are submitted to stresses and suffer deformations.

From 1 to 3 ms, the pressure decreases in the central area because the bubble gas starts coming out of the confined central zone. The maximum fluid speeds are recorded in the free space between the neutron shielding and the in-pile shell: around 90 m/s. The pressure decreases in the CCP too because the water thrown upwards flows out of the plug by the perforated part of the CCP external cylinder (this part is located between the upper spacer plate and the lower heat-insulation plate).

The water under the diagrid continues impacting the main vessel bottom and then flows along the vessel in direction of the collar. Consequently, a pressurised area forms under the Core Support Structure. The water below the internal vessel, after having rebounded against the collar, moves up towards and in the channel between the two vessels.

Between the CCP and the internal vessel, the bubble hurls water violently towards the small and large rotating plugs, towards the internal vessel intermediate and upper parts and in the space between the neutron shielding and the baffle. At 3 ms, a pressurised area creates along the internal vessel. The water flows lead to a compression and a concentration of the argon in the top corner: a pressure peak of 8 MPa is recorded at the junction with the main vessel.

During this time interval, the neutron shielding reaches a maximum opening of 64 mm, a maximum stress of 650 MPa at the top and a maximum plastic strain of 40 %. The baffle moves away of 37 mm at mid-height and suffers a plastic strain of 35 %. The top of the lower part of the internal vessel moves away until a maximum displacement of 18 mm. The diagrid support and the main vessel bottom continue their downward displacement. The CCP in-pile shell and spacer plates continue their upward motion because of the effect of the fluid thrust at the junction with the heat-insulation plate. Owing to the fluid splashing against the top closure, the small rotating plug begins going up.

Between 3 and 5 ms, the pressurised area along the internal vessel is propelled upwards. Pressure peaks are noted below the top closure: 5.5 MPa and 7 MPa at 3.5 ms at the centre and at the extremity of the heat-insulation plate, 7.5 MPa and 6.5 MPa at 4 ms under the small and large rotating plugs.

The bubble going out of the central area expands between the CCP and the internal vessel. It pushes water upwards along the CCP and the internal vessel upper part. The maximum speeds are now located out of the central area, in the bubble panache expanding in the mock-up. The argon starts orienting from the top corner to the channel between both vessels. The water below the internal vessel rebounds on the main vessel and goes back towards the intermediate part of the internal vessel. Meanwhile the water below the diagrid and the CSS is pushed back by the collar presence and orients towards the diagrid.

Besides of the previous structure deformations, we can observe a bending of the lower CCP heat-insulation plate, the complete crushing of the external cylinder bulge against the top closure, an upward displacement of the large rotating plug and the bending of the intermediate part of the internal vessel.

Maximum vertical displacements are reached in the main vessel at about 4 ms: -21 mm at the bottom and -10 mm at the junction with the collar. The diagrid support presents a maximum vertical displacement of -31 mm at 3.5 ms. The formation of the main vessel upper bulge and of the internal vessel upper bulge begins around 5 ms.

From 5 to 8 ms, the bubble gas goes on expanding out of the central zone. The size of the bubble panache is maximum at 8 ms, just before the formation of the whirlpool between the CCP and the internal vessel. The water below the diagrid moves along the main vessel from the collar to the diagrid, thus causing a going back of the diagrid support.

Below the internal vessel, the water moves upwards along the main vessel and impacts the intermediate part of the internal vessel. In the channel, the water goes up at the base while the argon goes down at the top, thus causing the formation of the main vessel upper bulge. As the argon pressure is higher than the water one, the bulge goes down following the going down of the argon in the channel.

The bubble gas continues propelling water against the internal vessel upper part, what induces a maximum radial displacement of 9.7 mm at the top at 7 ms and 11.5 mm at the upper bulge level at 7.5 ms.

From 8 to 13 ms, a whirlpool forms between the CCP and the internal vessel. The bubble panache stops its progression due to the resistance of the compressed water and turns round itself. This twirling movement pulls water from the top closure and from along the internal vessel. Argon and water are attracted from below the small rotating plug to the CCP and the fluid flow inside the CCP reverses.

The argon inserted in the channel between the vessels continues its downward progression and pushes down the water inside the channel as well as the water lower along the main vessel. The main vessel upper bulge moves down and reaches a maximum amplitude at 12 ms.

The water under the diagrid and the CSS slows down. Due to the water flow reversal in the mock-up bottom, the downward displacements of the main vessel and of the diagrid support come back from 4 to about 13 ms. The upward displacement of the top closure reaches a maximum value around 9 ms: 18 mm for the small rotating plug, 16 mm for the large plug, 11 mm for the roof at mid-length. Afterwards these upwards motions decrease because the whirlpool pulls the fluid instead of pushing it. However we observe a second pressure peak under the top closure at 10 ms, at the time of flow rebound and reversal on the top closure.

Between 14 and 17 ms, the whirlpool becomes independent from the rest of the fluid: it twirls on its own axis in the middle of water. No more bubble gas goes out from the central area. On the contrary, the whirlpool hurls back water and bubble gas inside the central area. These fluids impact violently the diagrid support and push up a bit more the in-pile shell. The fluid speeds become high again in the central area: up to 100 m/s.

The argon bag expands in the channel, along the top closure and in the CCP. The structure displacements remain constant in some cases (neutron shielding, internal vessel) or increase again in other cases (diagrid support, in-pile shell, main vessel bottom, top closure).

Later, the alternate fluid and structure motions are probably continuing because of the fluid rebounds against the structures. But progressively the fluid flows and the displacement amplitude will probably decrease and oscillate around stable location.

5 COMPARISON WITH THE EXPERIMENTAL RESULTS AND WITH PREVIOUS NUMERICAL RESULTS

The purpose of our computations consists in qualifying the CASTEM-PLEXUS code for the computation of Core Disruptive Accidents and to estimate the progress realised in the modeling of the accident. Thus the current numerical results are compared with the experimental results and previous numerical results computed with the CASTEM-PLEXUS code (Cariou, 1993). The main differences with the previous CASTEM-PLEXUS computations lay on the mesh fineness (Fig. 5) and the treatment of the fluid-structure coupling.

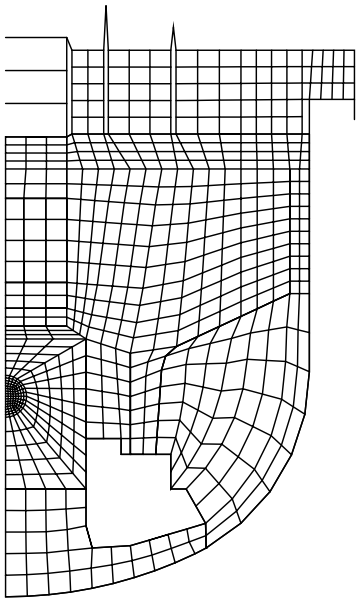

Fig. 5: Mesh used in the previous CASTEM-PLEXUS computation

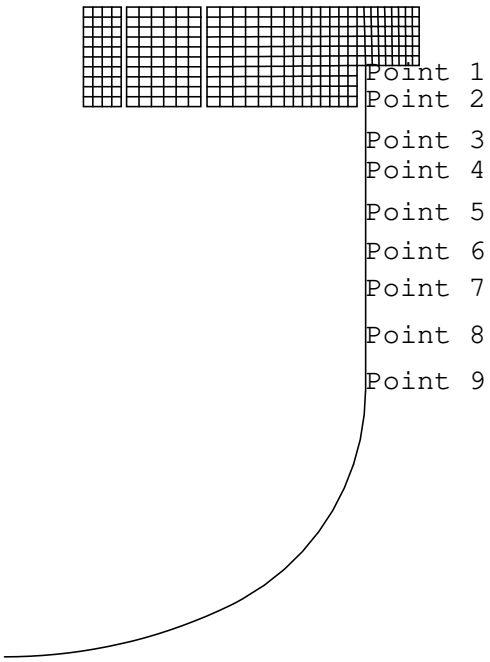

Fig. 8: Location of the points used to describe the main vessel upper bulge

The comparison concerns:

- the vertical displacement of the main vessel base,
- the radial displacement of the main vessel at the junction with the collar,
- the hoop strain of the vessel upper bulge,
- the vertical displacement of the roof,
- the vertical displacement of the diagrid support,
- the vertical displacement of the in-pile shell,
- the radial displacement of the lateral neutron shielding,
- the radial displacement of the baffle top,
- the radial displacement of the internal vessel at the top of the lower part and at the bulge level in the upper part,
- the impact pressure under the large rotating plug and under the roof and the instant of maximum.

The figures 6, 7 and 9 to 14 present respectively the vertical displacements of the main vessel at the bottom and at the junction with the collar, of the CCP heat-insulation lower plate, of the small and large rotating plugs, of the roof, of the diagrid support and of the CCP in-pile shell. The figures 15 to 19 show the radial displacements of the upper bulge of the main vessel, of the neutron shielding, of the baffle and of the internal vessel (lower and upper parts). The figures 20 to 22 display the pressure under the top closure. The table 1 presents a synthesis of the results.

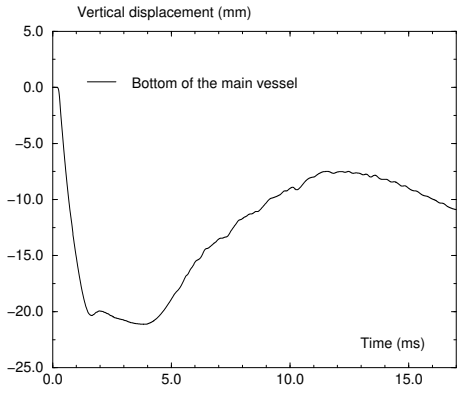

Fig. 6: Vertical displacement at the bottom of the main vessel

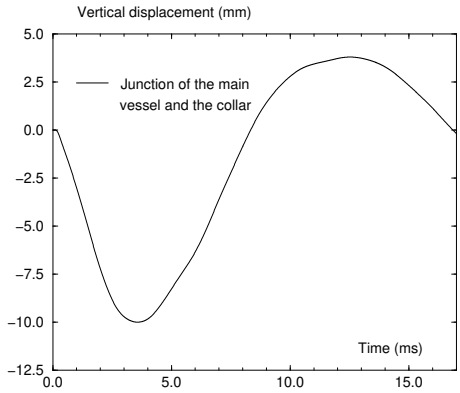

Fig. 7: Vertical displacement of point at the junction between the main vessel and the collar

Regarding the behaviour of the main vessel, the prediction of the new computations is downright better for the bottom displacement. Compared with the experimental results, the new computed displacements present an error of 50 % for the maximum value and 22 % at the end whereas the old predictions presented errors of about 150 %. At the junction with the collar, the computer displacements have not changed and still present an error of 66 %.

Concerning the upper bulge, the figure 8 displays the points where were recorded the evolution of the displacement versus time in the new CASTEM-PLEXUS computation. The comparison with the experimental data and with the previous computation concerns the area of the points 3 and 4. So the new computed result is more or less the same as the old computed one. It shows a discrepancy of about 100 % with the experimental one.

However, with the new simulation, we observe a going down of the fluid inside the channel between both vessels and the upper bulge follows the going down of the inner fluid. The maximum radial displacement is recorded for the points 5 and 6, just above the bottom of the channel. In the previous simulation, the upper bulge stayed located at the top of the mock-up, just under the roof: in the absence of several element layers in the channel, the FS2D coupling did not allow large fluid flows in the channel.

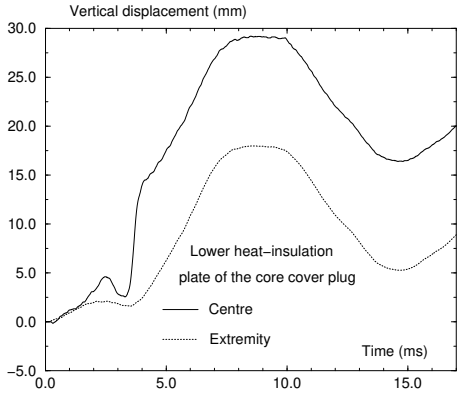

Fig. 9: Vertical displacement of the CCP heat-insulation lower plate

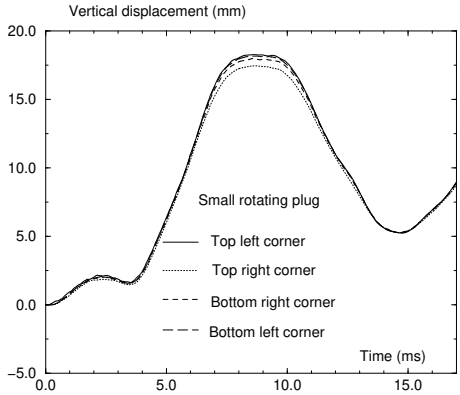

Fig. 10: Vertical displacement of the small rotating plug

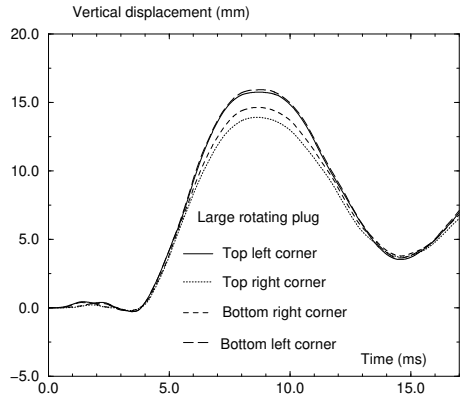

Fig. 11: Vertical displacement of the large rotating plug

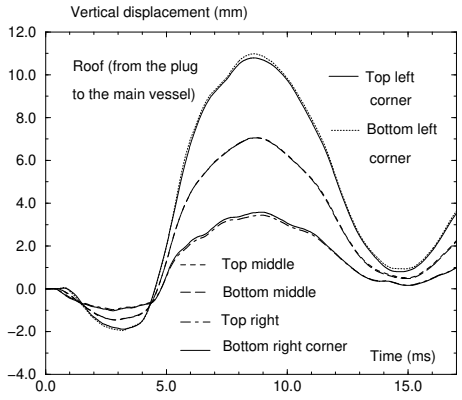

Fig. 12: Vertical displacement of the roof

About the vertical displacement of the top closure, the maximum value is computed in the small rotating plug. It is almost identical in the whole plug and around 17 - 18 mm. The displacement of the large rotating plug is a bit lower : between 14 and 16 mm. In the roof the maximum displacement is noted at the junction with the large rotating plug and is around 11 mm. At mid-distance between the plug junction and the main vessel, the displacement reaches a maximum of 7 mm whereas near the vessel the maximum value is no more than 3.5mm. The values noted in the different components confirm the deformation in stairs of the top closure with a vertical gap of some millimetres between two massive components.

For the comparison of the vertical displacement of the roof, we suppose that the concerned point is the one located on the roof at the joining ring limit with the rotating plug. The new results are a bit better than the old CASTEM-PLEXUS results but they remain far from the experimental results regarding the maximum displacement (100 % error). However the final displacement is quite correct.

Concerning the diagrid support displacement, we note a maximum displacement of 31 mm at 3.5 ms and a final displacement in the range 15 - 20 mm after 12 ms. The computed final value seems to be a bit better than the old CASTEM-PLEXUS one. As the old calculation lasted 20 ms of physical time whereas the new one was stopped at 17 ms, the conclusion about the improvement of the result is not sure.

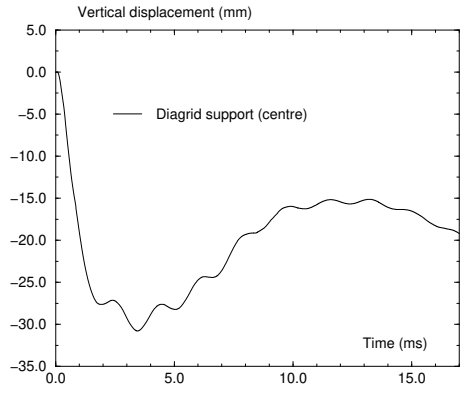

Fig. 13: Vertical displacement of the diagrid support

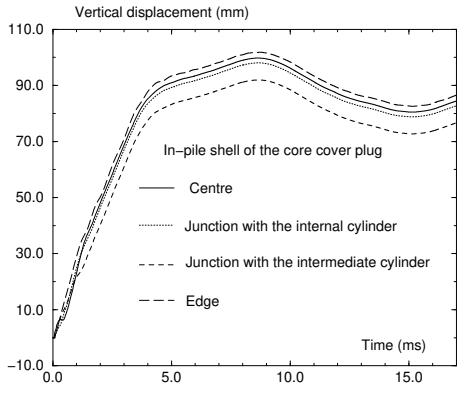

Fig. 14: Vertical displacement of the CCP in-pile shell

The comparison of the CCP in-pile shell vertical displacement shows, on the contrary, a neat improvement of the result precision. The error between the computed result and the experimental one fell from 28 % to 9 %. The reason of this improvement comes from the mesh fineness. In the new simulation, the mesh fineness is twice the one of the old computation. Consequently, in the new simulation, the CCP shells seems much more flexible than in the old simulation. The buckling of the external cylinder is more marked and thus the vertical displacement of the whole core cover plug is increased.

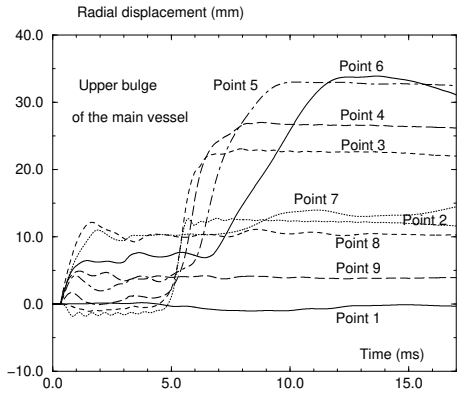

Fig. 15: Radial displacement of the upper bulge on the main vessel

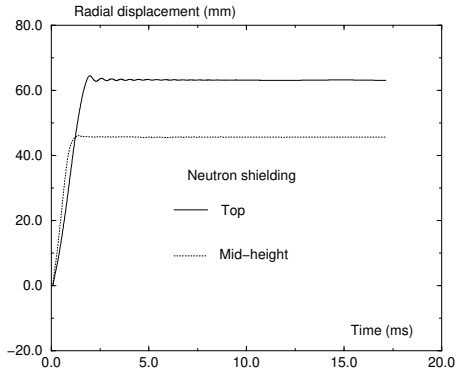

Fig. 16: Radial displacement of the neutron shielding

The radial displacement of the lateral neutron shielding top is higher than the one computed previously. But, in that case, the prediction is less precise than the old one. If the old prediction was almost exact, the new one presents 24 lines of shielding was represented in the simulation and thus the single shell is less rigid than the set of four shieldings.

Concerning the baffle radial displacement, the new simulation shows an error of 53 %. It is difficult to compare the old and new predictions because, in the old one, the baffle was completely blocked from the base to mid-height while, in the new simulation, the baffle can move freely. Considering that condition, it is normal to observe a larger displacement in the new simulation than in the old one.

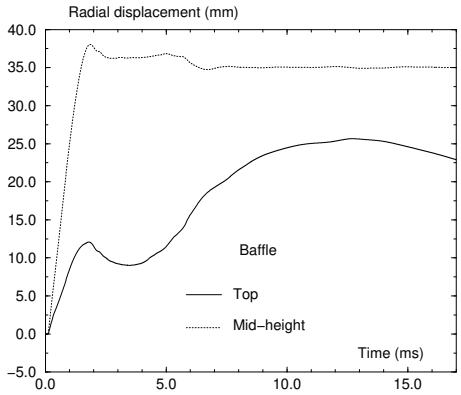

Fig. 17: Radial displacement of the baffle

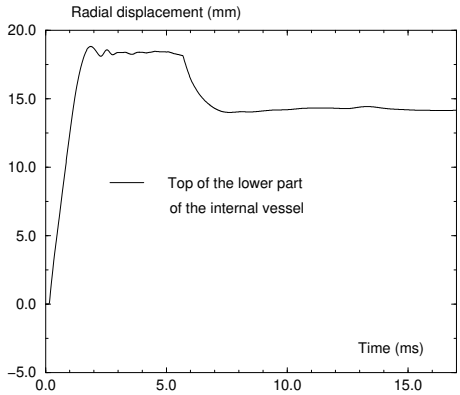

Fig. 18: Radial displacement of the top of the internal vessel lower part

Regarding the radial displacements of the internal vessel, the new simulation is in a better agreement with the experiment than the old simulation. In the new simulation, the results fit exactly for the prediction of the displacement at the top of the lower part of the internal vessel

as well for the maximum value as for the final value, and also for the prediction of the bulge formed in the upper part of the internal vessel.

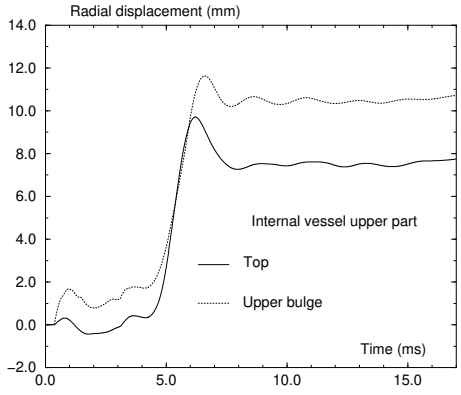

Fig. 19: Radial displacement of internal vessel upper part

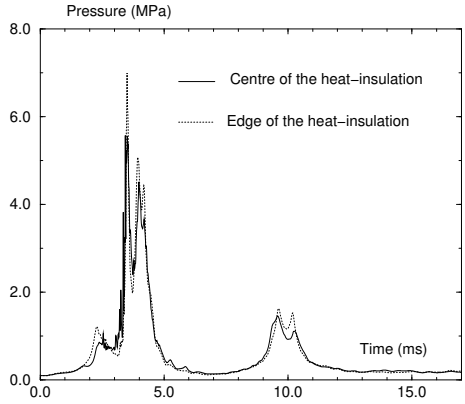

Fig. 20: Pressure under the CCP

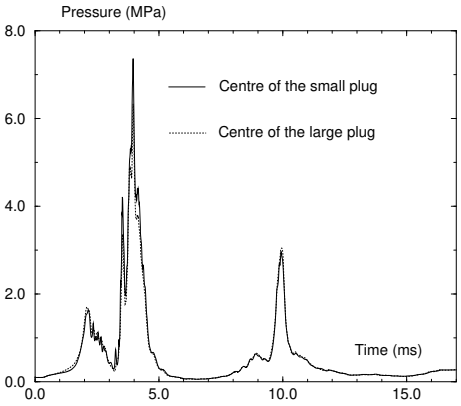

Fig. 21: Pressure under the two rotating plugs

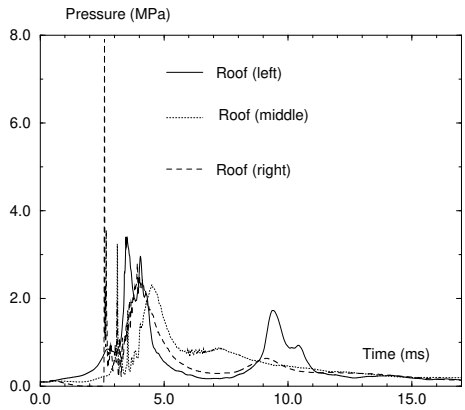

Fig. 22: Pressure under the roof

About the pressure peaks observed under the top closure, the new simulation is more precise than the old one. Even if the pressure level computed by CASTEM-PLEXUS remains much lower than the measured one (3.6 MPa instead of 19.4 MPa under the large rotating plug and 3.4 MPa instead of 5.4 MPa under the roof), the new simulation computes pressures equal to twice the previous computed ones. Besides, the instant of maximum is more precise for the pressure under the roof.

In the simulation, we can observe a high pressure peak up to 8 MPa in the corner formed by the roof and the main vessel. This peak value is approximately twice the average pressure elsewhere under the top closure due to the rebound of the shock wave against the wall.

Globally, the new simulation is in a better agreement than the old one, except regarding the prediction of the lateral neutron shielding and the baffle radial displacements. In the new simulation, the structure displacements and deformations are higher. That comes, at once, from the mesh refining because the structures meshed finely seem to be more flexible than with rough mesh and from the FSA coupling which allows tangential fluid flows along the shells.

In some cases, the new predictions fit very well with the experimental measures: in the case of the final roof displacement and of both upper and lower part internal vessel radial displacements. Nevertheless, the computed results would worth some more improvement for many structures.

6 CONCLUSION

In that paper, we present a computation of a Hypothetical Core Disruptive Accident in the MARS test-facility which is a small scale replica of a Fast Breeder Reactor. This mock-up contains all the internal structures of the reactor block. The fluids intervening in the real accident were replaced by water, argon and an explosive charge in the experiment.

In the numerical model, the majority of the structures are represented by shells or massive structures. However, the internal structures of complex geometry in the area of the internal vessels are simply taken into account by a pressure loss. The internal fluids are described by the specific CDA constitutive law implemented on purpose in the CASTEM-PLEXUS code for computing this kind of explosion.

The explosive wave propagates from the centre of the mock-up towards the main vessel and the top closure. The passing of the pressure wave loads and deforms the internal structures and then the external ones. The structures most in demand are the neutron shielding and the core cover plug because of their proximity with the pressurised area.

The high pressure gas bubble in the central part of the mock-up expands in the rest of the test-facility, thus pushing away the top of the neutron shielding and the in-pile shell. The argon layer under the top closure is pushed below the roof and in the channel between the internal and main vessels. A bulge forms in the upper part of the main vessel during the passing of the pressurised fluid in the channel.

During the explosion, the water contained into the mock-up is accelerated and hurled against the structures. In particular, the water impacts perpendicularly the main vessel and the top closure. The water thrust leads to a large deformation of the main vessel bottom. The fluid impacting the top closure causes a deformation in stairs (more important at the centre than at the edge) linked to the lower rigidity of the joining rings linking the massive slabs (plugs and roof).

A comparison of the computed results was performed with the experimental results, as well as previous results issued from the code CASTEM-PLEXUS. The main difference between both CASTEM-PLEXUS models lays in the treatment of the fluid-structure coupling and the mesh refinement. The results showed that the current model is in a better agreement with the MARS results than the old model. However, the simulation still shows some discrepancies which might come from the simplified modeling of the peripheral components.

In order to predict the influence of the peripheral structures (pumps, heat exchangers) acting as porous barriers and consequently having a protective effect on the containment by absorbing energy and slowing down the fluid impacting the containment, we developped in CASTEM-PLEXUS a new HCDA model taking into account the presence of the internal structures (without meshing them) by means of an equivalent porosity method (Robbe[b], 1999) (Robbe[c], 1999). This model has been applied to predict the MARS test.

REFERENCES

Acker, D., Benuzzi, A., Yerkess, A., Louvet, J., August 1981. MARA 01/02 - Experimental validation of the SEURBNUK and SIRIUS containment codes, Proc. 6th Int. Conf. on Structural Mechanics In Reactor Technology, Section E 3/6, Paris, France.

Albertini, C., et al. The JRC-COVA programme: Final Report. Commission of the European Communities, Report EUR 8705, 1983. Nuclear Science and Technology, 1984, pp. 1-182.

Benuzzi, A., 1987. Comparison of different LMFBR primary containment codes applied to a benchmark problem, Nuclear Engineering and Design 100, 239-249.

Blanchet, Y., Obry, P., Louvet, J., August 1981. Treatment of fluid-structure interaction with the SIRIUS computer code, Proc. 6th Int. Conf. on Structural Mechanics In Reactor Technology, Section B 8/8, Paris, France.

Bour, C., Spérandio, M., Louvet, J., Rieg, C., August 1989. LMFBR's core disruptive accident. Mechanical study of the reactor block, Proc. 10th Int. Conf. on Structural Mechanics In Reactor Technology, Vol. E, Anaheim, pp. 281-287.

Cameron, I.G., Hankin, B.C., Warham, A.G.P., Benuzzi, A., Yerkess, A., August 1977. The computer code SEURBNUK-2 for fast reactor explosion containment safety studies, Proc. 4th Int. Conf. on Structural Mechanics In Reactor Technology, Section B 2/1, San Francisco, USA.

Cariou, Y., Spérandio, M., Lepareux, M., Christodoulou, K., August 1993. LMFBR's whole core accident. Validation of the PLEXUS code by comparison with MARA tests, Proc. 12th Int. Conf. on Structural Mechanics In Reactor Technology, Section E 7/4, Stuttgart, Germany.

Cariou[a], Y., Pirus, J.P., Avallet, C., August 1997. LMR large accident analysis method, Proc. 14th Int. Conf. on Structural Mechanics In Reactor Technology, Section P 3/7, Lyon, France, pp. 395-402.

Cariou[b], Y., Lepareux, M., Noé, H., August 1997. LMR's whole core accident. Validation of the PLEXUS code by comparison with MARS test, Proc. 14th Int. Conf. on Structural Mechanics In Reactor Technology, Section P 2/6, Lyon, France, pp. 339-346.

Casadei, F., Daneri, A., Toselli, G., August 1989. Use of PLEXUS as a LMFBR primary containment code for the CONT benchmark problem, Proc. 10th Int. Conf. on Structural Mechanics In Reactor Technology, Section E 13/1, Anaheim, pp. 299-304.

Chang, Y.W., Gvildys, J., Fistedis, S.H., 1974. Analysis of the primary containment response using a hydrodynamic-elastic-plastic computer code, Nuclear Engineering and Design 27, 155-175.

Chang, Y.W., 1977. Application of containment codes to LMFBRs in the United States, Nuclear Engineering and Design 42, 53-67.

Chavant, C., Hoffmann, A., Verpeaux, P., Dubois, J., 1979. Plexus: A general computer code for explicit Lagrangian computation, Proc. 5th Int. Conf. on Structural Integrity In Reactor Technology, Section B 2/8, Berlin, Germany.

Cigarini, M., Daneri, A., Toselli, G., August 1983. Applications of ASTARTE-4 code to explosive models with complex internal structure using the rezoning facility, Proc. 7th Int. Conf. on Structural Mechanics In Reactor Technology, Section B 9/3, Chicago, USA.

Cowler, M.S., Hancock, S.L., 1979. Dynamic fluid-structure analysis of shells using the PISCES 2 DELK computer code, Proc. 5th Int. Conf. on Structural Mechanics In Reactor Technology, Section B 1/6, Berlin, Germany.

Daneri, A., Toselli, G., Trombetti, T., Blanchet, Y., Louvet, J., Obry, P, August 1981. Influence of the representation models of the stress-strain law on the LMFBR structures in an HCDA, Proc. 6th Int. Conf. on Structural Integrity In Reactor Technology, Section E 4/4, Paris, France.

David, F., 1978. Etude d'une composition explosive flegmatisée. Applications à la déformation d'une cuve, Proc. Symposium sur les hautes pressions dynamiques, Paris, France.

Falgayrettes, M., Fiche, C., Granet, P., Hamon, P., Barrau, P., Magnon, B., Jalouneix, J., Nédélec, M., 1983. Response of a 1/20 scale mock-up of the Superphenix breeder reactor to an HCDA loading simulation, Proc. 7th Int. Conf. on Structural Mechanics In Reactor Technology, Section E 4/1, Chicago, USA, pp. 157-166.

Fiche, C., Louvet, J., Smith, B.L., Zucchini, A., August 1985. Theoretical experimental study of flexible roof effects in an HCDA's simulation, Proc. 8th Int. Conf. on Structural Integrity In Reactor Technology, Section E 4/5, Brussels, Belgium, pp. 139-144.

Graveleau, J.L., Louvet, P., August 1979. Calculation of fluid-structure interaction for reactor safety with the CASSIOPEE code, Proc. 5th Int. Conf. on Structural Mechanics In Reactor Technology, Section B 1/7, Berlin, Germany.

Hoffmann, A., Lepareux, M., Schwab, B., Bung, H., 1984. Plexus - A general computer program for fast dynamic analysis, Proc. Conference on Structural Analysis and Design on Nuclear Power Plant, Porto Alegre, Brazil.

Holtbecker, H., 1977. Testing philosophy and simulation techniques, Nuclear Engineering and Design 42, 75-87.

Hoskin, N.E., Lancefield, M.J., 1978. The COVA programme for the validation of computer codes for fast reactor containment studies, Nuclear Engineering and Design 46, 17-46.

Idel'Cik, I.E., 1986. Memento des pertes de charge. Coefficients de pertes de charge singulières et de pertes de charge par frottement, Collection de la Direction des Etudes et Recherche d'EDF, Eyrolles, Paris, France, p. 362.

Kendall, K.C., Benuzzi, A., 1980. The COVA programme : Validation of the fast reactor containment code SEURBNUK, Nuclear Engineering and Design 57, 79-105.

Kendall, K.C., Adnams, D.J., 1986. Experiments to validate structural dynamics code used in fast reactor safety assessment, Science and Technology of Fast Reactor Safety, Vol. 2, British Nuclear Energy Society, London, England.

Lepareux, M., Bung, H., Combescure, A., Aguilar, J., August 1991. Analysis of a CDA in a LMFBR with a multiphasic and multicomponent behaviour law, Proc. 11th Int. Conf. on Structural Mechanics In Reactor Integrity, Section E 13/1, Tokyo, Japan, pp. 371-376.

Lepareux, M., Bung, H., Combescure, A., Aguilar, J., Flobert, J.F., August 1993. Analysis of an HCDA in a fast reactor with a multiphase and multicomponent behavior law, Proc. 12th Int. Conf. on Structural Mechanics In Reactor Integrity, Section E 7/2, Stuttgart, Germany, pp. 197-202.

Louvet, J., Hamon, P., Smith, B.L., Zucchini, A., August 1987. MARA 10: an integral model experiment in support of LMFBR containment analysis, Proc. 9th Int. Conf. on Structural Mechanics In Reactor Integrity, Section E, Lausanne, Switzerland, pp. 331-337.

Louvet., J., August 1989. Containment response to a core energy release. Main experimental and theorical issues - Future trends, Proc. 10th Int. Conf. on Structural Mechanics In Reactor Integrity, Vol. E, Anaheim, pp. 305-310.

NERSA, 1987. The Creys-Malville power plant, Electricité de France, Direction de l'équipement, Région d'équipement Alpes-Lyon, France.

Robbe, M.F., Lepareux, M., Bung, H. Plexus - Notice théorique, CEA report DMT/94-490, 1994.

Robbe[a], M.F., Galon, P., Yuritzinn, T., November 1999. Castem-Plexus: Un logiciel de dynamique rapide pour évaluer l'intégrité des structures en cas d'accident, Proc. 4th Conf. INSTRUC, Courbevoie, France.

Robbe[b], M.F., August 1999. A porosity method to model the internal structures of a reactor vessel, Proc. 15th Int. Conf. on Structural Mechanics In Reactor Technology, Vol. B, Seoul, Korea.

Robbe[c], M.F., Bliard, F., April 1999. A porosity model to represent the influence of structures on a fluid flow. Application to a hypothetical core disruptive accident, Proc. 7th Int. Conf. On Nuclear Engineering, paper 7819, Tokyo, Japan.

Sidoli, J.E.A., Kendall, K.C. The WINCON programme - Validation of the fast reactor primary containment codes. Proc. INE Int. Conf. On Nuclear Containment, Cambridge, England, April 1987. Nuclear Containment Structures, D.G. Walton, Cambridge University Press, 1988.

Smith, B.L., Yerkess, A., Adamson, J., August 1983. Status of coupled fluid-structure dynamics code SEURBNUK, Proc. 7th Int. Conf. on Structural Mechanics In Reactor Technology, Section B 9/1, Chicago, USA.

Smith, B.L., Fiche, C., Louvet, J., Zucchini, A., August 1985. A code comparison exercise based on the LMFBR containment experiment MARA-04. Proc. 8th Int. Conf. on Structural Mechanics In Reactor Technology, Section E 4/7, Brussels, Belgium, pp. 151-157.

Smith B.L., Yerkess, A., Washby, V., August 1987. The computer code SEURBNUK-EURDYN: First release version, Proc. 9th Int. Conf. on Structural Mechanics In Reactor Technology, Lausanne, Switzerland.

Stiévenart, M., Bouffioux, P., Eglème, M., Fabry, J.P., Lamotte, H. August 1975. Analysis of LMFBR explosion model experiments by means of the Surboum-II code, Proc. 3rd Int. Conf. on Structural Mechanics In Reactor Technology, Section E 3/5, London, England.

Wenger, H.U., Smith, B.L., 1987. On the origin of the discrepancies between theory and experiment in the COVA series, Proc. 9th Int. Conf. on Structural Mechanics In Reactor Technology, Vol. E, Lausanne, Switzerland, pp. 339-344.
West, P.H., Hoskin, N.E. APRICOT - Phase 3. Suggested simple test problems for examination of thin shell modelling and fluid structure coupling, Aldermaston report AWRE/44/92/16, 1980.

		Experiment		Old CP computations		New CP computations	
		Maximum	Final	Maximum	Final	Maximum	Final
Main vessel bottom	Vert. displacement (mm)	-14	-9	-34	-26	-21	-11
Junction main vessel-collar	Vert. displacement (mm)	-6		-10		-10	
Main vessel upper bulge	Hoop strain (%)	2.4	1.9	4.8	4.4	4.4	4.2
Roof	Vert. displacement (mm)	5.5	5	12	5	11	4
Diagrid support	Vert. displacement (mm)		-18		-23	-31	-20
CCP in-pile shell	Vert. displacement (mm)		97	70	70	102	88
Neutron shielding	Radial displacement (mm)	54	50		53	64	62
Baffle	Radial displacement (mm)		15		14	25	23
Internal vessel	Radial displacement (mm) of the lower part top	19	15		10	18.5	14
	Radial displacement (mm) of the upper part bulge		10		15	11.5	10.5
Pressure under the large rotating plug	Max. pressure (MPa)	19.4		3.6		6.4	
	Instant of max (ms)	3		3		4	
Pressure under the roof in the argon	Max. pressure (MPa)	5.4		2		3.4	
	Instant of max (ms)	4.1		7		4	

Table 1: Comparison between the experimental results and the results computed by CASTEM-PLEXUS